# Development of A Miniaturized Wideband 16-Way Power Divider Using Loaded Spurlines

Lingna Gu [1, a] , Zhiyuan Zong [1, b]

[1]School of Electronic and Optical Engineering, Nanjing University of Science and Technology, Nanjing210018, China.

[a] gu_lingna@163.com, [b] zongzhiyuan@sina.com

**Abstract.** A New wideband Wilkinson 16-way power divider on microstrip line operating at X-band(8-12GHz) using loaded slow-wave structure of spurline to accomplish miniaturization is presented in this paper.The equations used for the 2-way power divider unit loaded with symmetrical single-spurline structures are based on the concept of spurline and odd-even modes using transmission line analysis.Then the 2-way power divider in X-band is cascaded to design 16-way power divider, while every cascade transmission line is loaded with symmetrical-spurline structure.The designed 16-way power divider has compact size of 197 mm × 55.1 mm × 6.808 mm including cavity and provides good impedence matching at all ports.Its return loss is better than 12.98dB, insertion loss is less than 15.1dB and isolation is better than 15dB across the 8 to 12GHz range, which is in good agreement with the simulation results.

**Keywords:** 16-way power divider;Wilkinson power divider;Miniaturization;Wideband;Spurline.

## 1. Introduction

Phased arrays as electronically scanned array with significant advantages, have got more and more attention in radar, air borne and ground based applications[1]. Since phased array transmitter combines power from multiple channels, N-way feed network is required.In general, this feed is provided by the power divider[2].It is common that Wilkinson power divider has been used in phased array network, combiners, and array antenna networks because of its good phase and amplitude consistency and good isolation between the output ports. However, these dividers usually have narrow bandwidth.There are some methods to increase the bandwith[3].

As an efficient N-way power divider, it should provide equal power division, good phase consistency, high isolation, wide bandwidth and compact size[4]. Fig.1 shows two topologies which are used to design N-way power divider.

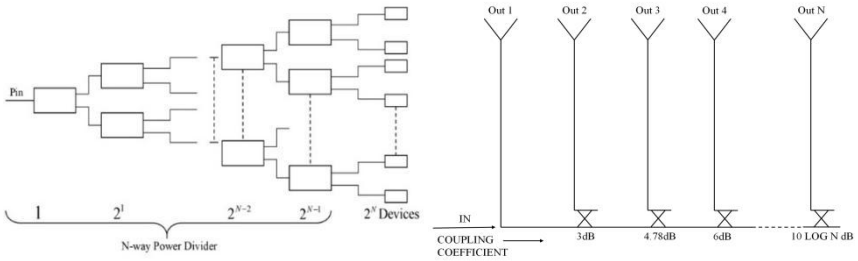


(a) (b)

Fig.1 (a)Tree structure(b)Chain structure

Compared with chain structure, the tree structure has the advantage of easy integration. In addition, bandwidth can be expanded effectively by choosing the appropriate length of cascade transmission lines. A 16-way X-band(8-12GHz) Wilkinson power divider using tree structure is presented in [5] with good performance. The only fly in the ointment is its large size.

In this paper, a new miniaturized wideband 16-way Wilkinson power divider is developed. Different from previous works, we load slow-wave structures of single-spurline and symmetrical-spurline on the microstrip lines to achieve miniaturization. The equivalent circuits are analyzed to assist the design procedure. Simulated results and experimental results are presented respectively. Conclusion is given in sixth part.

## 2. Analysis of 2-Way Power Divider Unit Using Loaded Spurlines

The proposed power divider design is based on a basic Wilkinson divider. Single divider is utilized in next stages in binary form for power division to get 16-way power divider. In the design, the configuration of a 2-way power divider unit using symmetrically loaded single-spurline structures is shown in Fig.2. Cutting angle bends are used in the proposed power divider to avoid the stray capacitance caused by the right-angled bends.

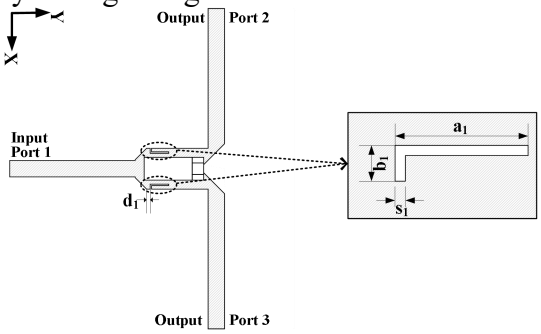


Fig. 2 2-way power divider using loaded spurlines

As shown in Fig.1, assume that the characteristic impedence of input transmission line is $Z_1$, and the characteristic impedence of the quarter wavelength transmission lines at port 2 and 3 are both $Z_2$ in order to get equal power division.Correspondingly, $Z_3$ represents the characteristic impedence of transmission lines at output port 2 and 3. A shunt chip fixed resistor *R* is then placed between the two uncoupled quarter wavelength transmission lines for isolation, which has 0603 package that is modeled properly in HFSS design. In general, the even- and odd-mode analysis is carried out to determine the structure parameters. On the assumption that input port 1 and output port 2 and 3 have terminal impedences of $Z_S$ and $Z_L$ respectively.

### 2.1 Even-Mode Analysis

The even-mode equivalent circuit is shown in Fig.3. For even-mode excitation, the isolation resistor *R* is equivalent to an open circuit since there is no current flows through.

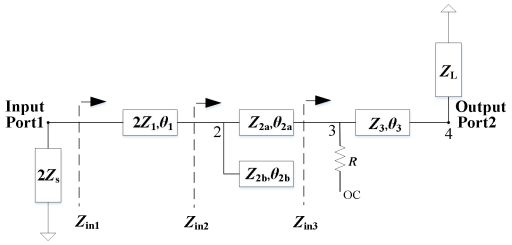


Fig. 3 Even-mode equivalent circuit

Based on the transmission line theory, the transition matrix between nodes 3 and 4 can be derived as below when the center matching frequency is $f$:

$$\begin{bmatrix} A_{4e} & B_{4e} \\ C_{4e} & D_{4e} \end{bmatrix} = \begin{bmatrix} \cos\theta_3 & \mathrm{j}Z_3\sin\theta_3 \\ \dfrac{\mathrm{j}\sin\theta_3}{Z_3} & \cos\theta_3 \end{bmatrix} \tag{a}$$

Thus the input impedence at node 3 can be obtained:

$$Z_{in3} = \frac{A_{4e}Z_L + B_{4e}}{C_{4e}Z_L + D_{4e}} \tag{b}$$

Likewise, the transition matrix between nodes 2 and 3 is as following:

$$\begin{bmatrix} A_{3e} & B_{3e} \\ C_{3e} & D_{3e} \end{bmatrix} = \begin{bmatrix} 1 & 0 \\ \frac{\mathrm{j}\tan\theta_{2b}}{Z_{2b}} & 1 \end{bmatrix} \begin{bmatrix} \cos\theta_{2a} & \mathrm{j}Z_{2a}\sin\theta_{2a} \\ \frac{\mathrm{j}\sin\theta_{2a}}{Z_{2a}} & \cos\theta_{2a} \end{bmatrix} = \begin{bmatrix} \cos\theta_{2a} & \mathrm{j}Z_{2a}\sin\theta_{2a} \\ \frac{\mathrm{j}\tan\theta_{2b}}{Z_{2b}}\cos\theta_{2a} + \frac{\mathrm{j}\sin\theta_{2a}}{Z_{2a}} & \frac{-Z_{2a}\sin\theta_{2a}\tan\theta_{2b}}{Z_{2b}} + \cos\theta_{2a} \end{bmatrix} \tag{c}$$

We can obtain the input impedence at node 2:

$$Z_{in2} = \frac{A_{3e}Z_{in3} + B_{3e}}{C_{3e}Z_{in3} + D_{3e}} \tag{d}$$

Then the transition matrix between nodes 1 and 2 is given:

$$\begin{bmatrix} A_{2e} & B_{2e} \\ C_{2e} & D_{2e} \end{bmatrix} = \begin{bmatrix} \cos\theta_1 & \mathrm{j}2Z_1\sin\theta_1 \\ \frac{\mathrm{j}\sin\theta_1}{2Z_1} & \cos\theta_1 \end{bmatrix} \tag{e}$$

And it is easy to derive the input impedence at node 1:

$$Z_{in1} = \frac{A_{2e}Z_{in2} + B_{2e}}{C_{2e}Z_{in2} + D_{2e}} \tag{f}$$

Consequently, the reflection coefficient at input port 1 can be calcultated:

$$\Gamma(\mathrm{in1}) = \frac{Z_{in1} - 2Z_S}{Z_{in1} + 2Z_S} \tag{g}$$

In order to guarantee good impedence matching in operating band, first of all, the maximum value of the reflection coefficient at input port 1 has to be minimised in the corresponding frequency band.

### 2.2 Odd-Mode Analysis

The odd-mode equivalent circuit is shown in Fig.4. For odd-mode excitation, the voltage equals to zero along the centre line of the equivalent circuit.

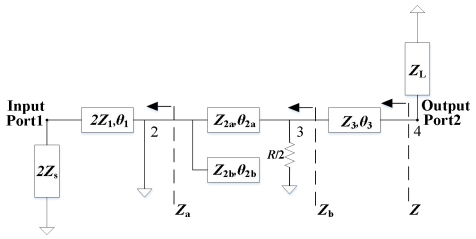


Fig. 4 Odd-mode equivalent circuit

In the same way, the transition matrix between nodes 3 and 2 can be derived as below when the center matching frequency is $f$:

$$\begin{bmatrix} A_{3o} & B_{3o} \\ C_{3o} & D_{3o} \end{bmatrix} = \begin{bmatrix} \cos\theta_{2a} & \mathrm{j}Z_{2a}\sin\theta_{2a} \\ \frac{\mathrm{j}\sin\theta_{2a}}{Z_{2a}} & \cos\theta_{2a} \end{bmatrix} \begin{bmatrix} 1 & 0 \\ \frac{j\tan\theta_{2b}}{Z_{2b}} & 1 \end{bmatrix} = \begin{bmatrix} \frac{-Z_{2a}\sin\theta_{2a}\tan\theta_{2b}}{Z_{2b}} + \cos\theta_{2a} & jZ_{2a}\sin\theta_{2a} \\ \frac{j\tan\theta_{2b}}{Z_{2b}}\cos\theta_{2a} + \frac{j\sin\theta_{2a}}{Z_{2a}} & \cos\theta_{2a} \end{bmatrix} \tag{h}$$

Hence the input impedence at node 3 can be obtained:

$$Z_b = \frac{\left(\frac{B_{3o}}{D_{3o}}\right)\frac{R}{2}}{\frac{B_{3o}}{D_{3o}} + \frac{R}{2}} \tag{i}$$

The transition matrix between nodes 4 and 3 is as following:

$$\begin{bmatrix} A_{4o} & B_{4o} \\ C_{4o} & D_{4o} \end{bmatrix} = \begin{bmatrix} \cos\theta_3 & jZ_3\sin\theta_3 \\ \frac{j\sin\theta_3}{Z_3} & \cos\theta_3 \end{bmatrix} \tag{j}$$

We can easily obtain the input impedence at node 4:

$$Z = \frac{A_{4o}Z_b + B_{4o}}{C_{4o}Z_b + D_{4o}} \tag{k}$$

Therefore, the reflection coefficient at output port 2 can be calcultated:

$$\Gamma(\text{in2}) = \frac{Z - Z_L}{Z + Z_L} \tag{l}$$

It is also crucial that the maximum value of the reflection coefficient at output port 2 has to be minimised in the corresponding frequency band to achieve good impedence matching.

In addition, the resistence of the isolation resistor can be obtained through the analysis of odd-mode equivalent circuit. When the reflection coefficient reaches the optimum value, the isolation meets the requirements meanwhile.

## 3. Design of Miniaturized Wideband 16-Way Power Divider

The proposed 16-way power divider operating at centre frequency of 10GHz with equal power division is fabricated on low loss Rogers 4350B substrate with relative permittivity of 3.66, loss tangent of 0.004 and thickness of 0.508mm, which covers the whole operating band from 8GHz to 12GHz. Input port takes feed from SMA coaxial connector and output ports take feed from SMP coaxial connectors.The chip fixed isolation resistors are in 0603 package form.Cutting angle bends used in the proposed power divider are shown in Fig.5.

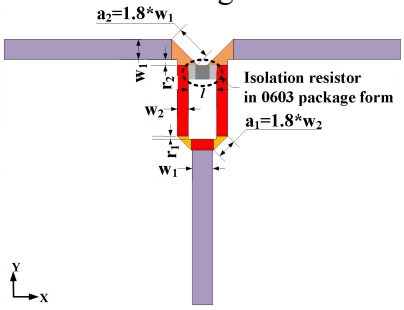


Fig. 5 Cutting angle bends in detail

The parameters of cutting angle bends can be calculated as :

$$a_1 = 1.8 * w_2 \tag{m}$$

$$r_1 = \frac{1.8 * w_2}{\sqrt{2}} - w_2 \tag{n}$$

$$a_2 = 1.8 * w_1 \tag{o}$$

$$r_2 = \frac{1.8 * w_1}{\sqrt{2}} - w_1 \tag{p}$$

$a_1$ and $a_2$ are preferred according to engineering experience, where $w_1$ is the width of input and output transmission lines since the power division ratio is 1 and $w_2$ is the width of quarter wavelength transmission lines. The characteristic impedences $Z_1$, $Z_2$ and $Z_3$ are chosen to be 50Ω, 70.7Ω and 50Ω respectively. Then the isolation resistor is calculated to be 100Ω. Length and width of microstrip lines can be calculated by entering known parameters using Txline software.

2-way power dividers are used in cascade to get 16-way power divider. Therefore, we load symmetrical single-spurline structures on the quarter wavelength impedence transformer of every X-band 2-way power divider unit to accomplish miniaturization at first. Then we load symmetrical-spurline structure on every cascade transmission line along the Y-axis to further reduce the whole width of the 16-way power divider. Fig.6 shows the prototype of the miniaturized X-band 2-way power divider unit. We load additional symmetrical rectangular notch structures to compensate for the impedence mismatching caused by size reduction.

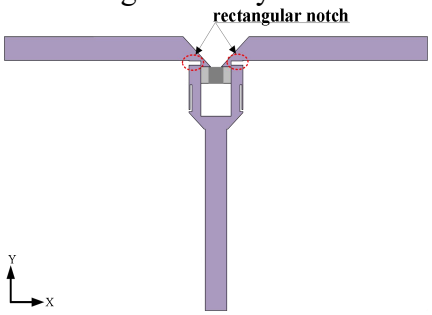


Fig. 6 Prototype of the miniaturized X-band 2-way power divider unit

This power divider unit is cascaded to form the 16-way power divider on the basis of the distance between two output ports set to be 12mm. The electrical length of every cascade transmission line is chosen as multiple of 90° before reduction because as phase is increased, the length of transmission line is increased and the effect of quarter wavelength remains the same.

After loading symmetrical-spurline structures on every cascade transmission lines along the Y-axis, optimizing all values and fine-tuning the whole model in simulation software HFSS. Fig.7 shows the plane structure of half of the miniaturized wideband 16-way power divider.The other part can be formed by duplicating. Magnifications of every stage of 2-way power divider are shown in Fig.8. Some open-circuited stubs in parallel are added to the transmission lines to optimize the circuit performance.

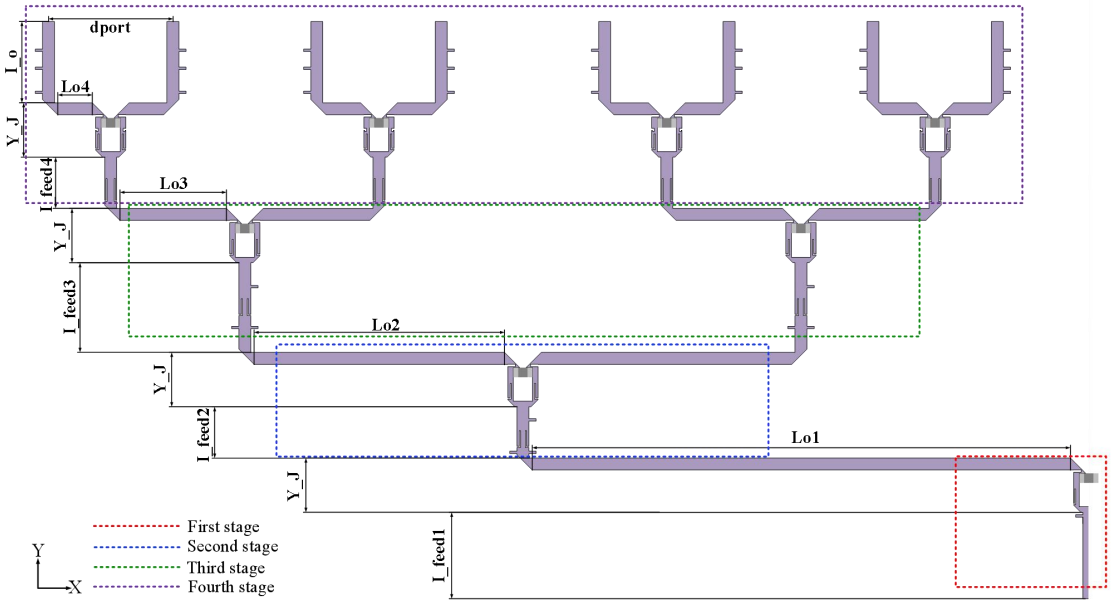


Fig. 7 Structure of half of the miniaturized wideband 16-way power divider

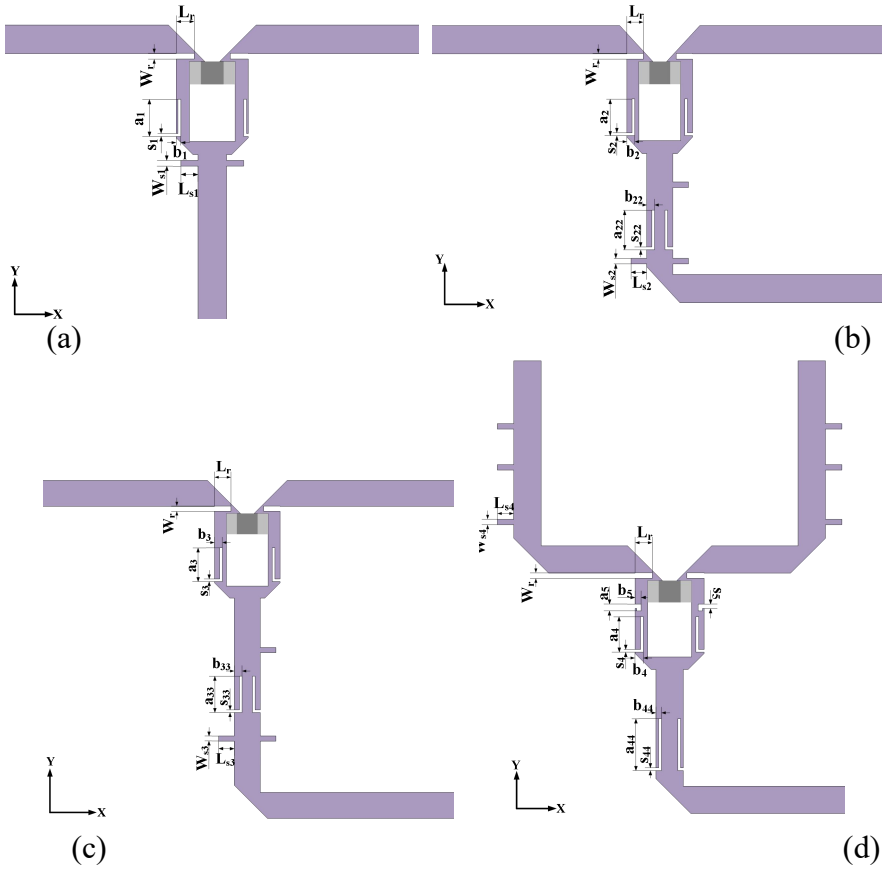


Fig.8 Magnifications of every stage of 2-way power divider
(a) First stage 2-way power divider (b) Second stage 2-way power divider
(c) Third stage 2-way power divider (d) Fourth stage 2-way power divider

Table 1. Shows the optimized values of the dimensions of the proposed miniaturized broadband 16-way power divider.

Table 1. Optimized dimensions of the miniaturized broadband 16-way power divider

| Parameter | Value(mm) | Variable | Value(mm) | Variable | Value(mm) |
|---|---|---|---|---|---|
| W | 191 | $b_1$ | 0.16 | $L_{s1}$ | 0.6 |
| L | 48.1 | $s_1$ | 0.1 | $W_{s2}$ | 0.2 |
| W1 | 1 | $a_2$ | 1.3 | $L_{s2}$ | 0.6 |
| W2 | 0.46 | $b_2$ | 0.3 | $W_{s3}$ | 0.2 |
| I_feed1 | 7.2 | $s_2$ | 0.1 | $L_{s3}$ | 0.6 |
| Lo1 | 44.88 | $a_3$ | 1.3 | $W_{s4}$ | 0.2 |
| I_feed2 | 4 | $b_3$ | 0.3 | $L_{s4}$ | 0.6 |
| Lo2 | 20.88 | $s_3$ | 0.1 | $a_{22}$ | 1.4 |
| I_feed3 | 7.2 | $a_4$ | 1.3 | $b_{22}$ | 0.3 |
| Lo3 | 8.88 | $b_4$ | 0.3 | $s_{22}$ | 0.1 |
| I_feed4 | 4 | $s_4$ | 0.1 | $a_{33}$ | 1.4 |
| Lo4 | 2.88 | $a_5$ | 0.25 | $b_{33}$ | 0.3 |
| I_o | 6.5 | $b_5$ | 0.22 | $s_{33}$ | 0.1 |
| r1 | 0.13 | $s_5$ | 0.16 | $a_{44}$ | 1.9 |
| r2 | 0.27 | $W_r$ | 0.2 | $b_{44}$ | 0.2 |
| Y_J | 4.8 | $L_r$ | 0.63 | $s_{44}$ | 0.1 |
| $a_1$ | 1.3 | $W_{s1}$ | 0.2 | | |

## 4. Simulated Results

This section presents simulated results of the optimized miniaturized broadband 16-way power divider. Fig.9 shows the simulated results.

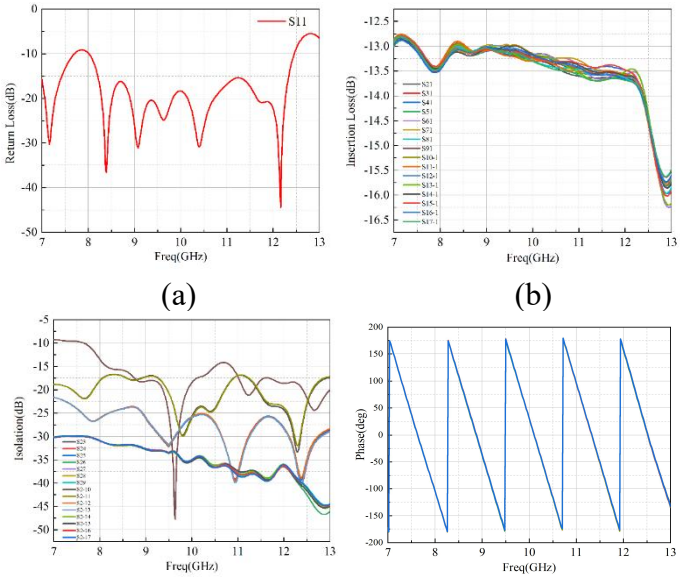


(a) (b)

(c) (d)

Fig. 9 Simulated results of the optimized miniaturized broadband 16-way power divider
(a) input return loss (b)insertion loss of each channel
(b) isolation between each channel (c)phase characteristics at each channel

Input port is considered as port 1 and output ports are considered as port 2 to 17 representing the 16 channels of power divider.As shown in Fig.9 (a), the proposed 16-way miniaturized power divider has good impedence matching from 8GHz to 12GHz, while the input renturn loss is less than -15dB. Insertion loss of each channel is shown in Fig.9 (b), which is better than 13.7dB within whole X-band. The worst value 13.68dB of insertion loss occurs at 11.44GHz. From Fig.9 (c), we can see the isolation curves are basically bellow -15dB across the 8 to 12GHz range, except for some slight upward shift from 8GHz to 8.14GHz and 10.48GHz to 10.87GHz. In addition, Fig.9 (d) shows that the deviation of phase between each channel is very small. It can be seen that the proposed miniaturized 16-way power divider has wideband performance, good impedence matching, renturn loss and isolation within the whole X-band.

## 5. Experimental Results

The simulated results are more close to the ideal situation. Given that actual machining factors can affect the experimental results, it is important to adjust the model to match the machining such as screwing the substrate to ground and surrounding the model with metal walls to fix coxial connectors. Fabricated figure of the final miniaturized wideband 16-way power divider are presented in Fig.10. It has the size of 197 mm × 55.1 mm × 6.808 mm including cavity and plan dimension of 191mm × 48.1 mm, which is only 10.91 $\lambda_g$ ×2.75 $\lambda_g$ . Fig.11 shows experimental results.

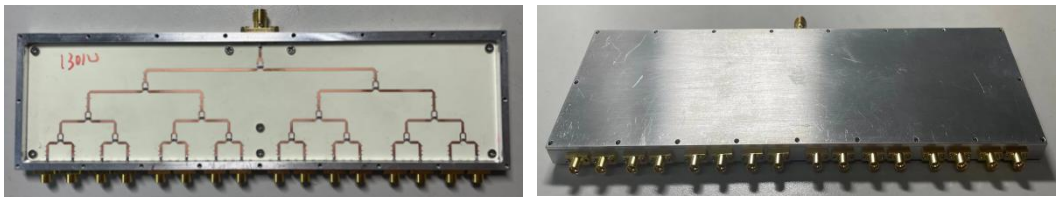

(a) (b)

Fig.10 Fabricated diagram of the miniaturized wideband 16-way power divider
(a)without cavity lid (b)with cavity lid

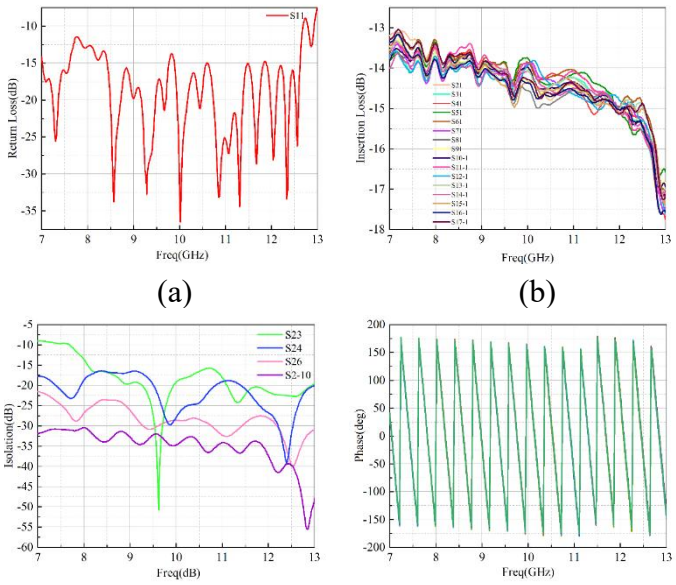


(a) (b)

(c) (d)

Fig.11 Fabricated results

(a)input return loss (b) insertion loss of each channel

(c) isolation between port 2 and port 3, 4, 6, 10 (d) phase characteristics at each channel

The measured input return loss are less than -12.98dB while the measured isolation is better than 15dB within the whole X-band. It is easy to find that the input return loss at 8GHz is even better in comparison with the simulated value, and the isolation curves from 10.48GHz to 10.87GHz are also below -15dB. Fig.11 (b) shows the insertion loss of each channel which is less than 15.1dB and increases over simulated value by 1.4dB. Fig.11 (d) demonstrates good phase consistency performance. All experimental results are much close to the simulated results. There are some variations inevitably caused by the loss of microstrip lines and manufacturing limitations.

## 6. Conclution

In this paper, a miniaturized wideband 16-way power divider using loaded spurlines is presented. The 2-way power divider unit has single section and is used in cascade to form the16-way power divider. The proposed 16-way power divider has compact size of 197 mm × 55.1 mm × 6.808 mm including cavity, good input and output return loss less than -12.98dB, insertion loss less than 15.1dB and isolation better than 15dB within the whole operating band from 8GHz to 12GHz. And good phase consistency makes it best choice for phase array transmitters as feed network.

## References

[1] Parker Don and David C. Zimmermann, "Phased Array - Theory and Architecture Part 1", IEEE Transaction on Microwave Theory and Techniques, vol. 50, no. 3, March 2002.

[2] Kwang-Jin Koh, Jason W. May and Gabriel M. Rebeiz, "A Millimetr wave (40 – 45GHz) 16 Element Phased Array Transmitter in 0.18 um SiGe BiCMOS Technology", IEEE Journal of Solid State Circuits, vol. 44, no. 5, May 2009.

[3] Seymour B. Kohn, "A Class of Broadband Three Port TEM Mode Hybrid", IEEE Transaction on Microwave Theory and Techniques, vol. MTT-16, no. 2, Feburary 1968.

[4] K. Chang and C. Sun, "Millimeter-Wave Power-Combing Techniques", IEEE Transactin Microwave Theory and Techniques., vol. MlT-31, no. 2, pp. 91-107, Feburary 1983.

[5] A. A. Rauf, J. Tahir, A. Raza, A. Ali and I. H. Umrani, "16 ways X-band wilkinson power divider for phased array transmitter," 2018 15th International Bhurban Conference on Applied Sciences and Technology (IBCAST), Islamabad, Pakistan, 2018, pp. 835-840.